Ab initio molecular dynamics simulations with linear scaling: application to liquid ethanol

2008 J. Phys.: Condens. Matter 20 294212

(http://iopscience.iop.org/0953-8984/20/29/294212)

IOP PUBLISHING JOURNAL OF PHYSICS: CONDENSED MATTER

J. Phys.: Condens. Matter **20** (2008) 294212 (7pp) doi:10.1088/0953-8984/20/29/294212

Ab initio molecular dynamics simulations with linear scaling: application to liquid ethanol

Eiji Tsuchida

Research Institute for Computational Sciences, National Institute of AIST, Tsukuba Central 2, Umezono 1-1-1, Tsukuba 305-8568, Japan

Received 9 January 2008
Published 24 June 2008
Online at stacks.iop.org/JPhysCM/20/294212

Abstract

The structural and dynamical properties of liquid ethanol (C_2H_5OH) at ambient conditions have been studied by *ab initio* molecular dynamics simulations using a large supercell containing 125 molecules (1125 atoms). The results obtained from a trajectory of 10 ps are found to be in good agreement with available experimental data. Without sacrificing accuracy, the computational cost of simulations is reduced by more than a factor of four by the linear scaling algorithm based on the augmented orbital minimization method.

S Supplementary data are available from stacks.iop.org/JPhysCM/20/294212

(Some figures in this article are in colour only in the electronic version)

1. Introduction

Ethanol is in wide commercial use in beverages, solvents, and fuels, making it one of the most important alcohols. Therefore much effort has been devoted to understanding the properties of liquid ethanol from numerical simulations. Most of the previous results have been obtained by molecular dynamics (MD) and Monte Carlo simulations using empirical interatomic potential functions [1–9]. The most widely used potential function for ethanol is the OPLS (optimized potential for liquid simulations) force field [1–4], while more elaborate potential functions have also been developed [5–9]. Overall, these simulations are able to reproduce the experimental features relatively well, suggesting that liquid ethanol at ambient conditions consists mainly of winding chains linked by O–H···O hydrogen bonds, in analogy with methanol. Nevertheless, different force fields give significantly different values for some properties like hydrogen-bond statistics [6] that are not available from experiments. In the absence of accurate reference data, however, there is no way to judge which force field is more reliable. Furthermore, united atom and rigid body approximations are used in many force fields, which makes the analysis of intramolecular properties difficult.

In contrast, the atomic forces are calculated directly from first principles without adjusting empirical parameters in the density-functional theory (DFT) [10–13], which allows us to investigate the intra- and intermolecular properties of condensed systems on an equal footing. *Ab initio* study of hydrogen-bonded liquids using DFT started with water in the early 1990s [14, 15], followed by ammonia [16–18], methanol [19–23], formamide [24], and phosphoric acid [25]. There are also many studies on the aqueous solutions of ions [26, 27]. As a result of these studies, DFT is considered to give satisfactory results for structural and dynamical properties of hydrogen-bonded liquids. While DFT has already been applied to aqueous solutions of ethanol [28], to the best of our knowledge there has been no *ab initio* study of liquid ethanol to date. This is mainly because we need of the order of 10^3 atoms to model the liquid phase of ethanol, which is computationally too expensive on today's computers.

Recently, a number of novel algorithms called linear scaling methods [29–47] have been proposed to improve the performance of large scale electronic structure calculations. In these methods, the computational cost of evaluating the total energy and atomic forces grows only linearly with system size by taking advantage of the nearsightedness principle [48]. In the meantime, a variety of real space basis sets, such as finite differences [49–52], finite elements [53–59], B-splines [60], spherical waves [61], and wavelets [62, 63], have been developed for DFT calculations in the last decade, some of which are already competitive with the conventional plane wave basis set in terms of accuracy and performance [64]. A prominent feature of real space basis functions is that they are exactly localized in real space, while exhibiting

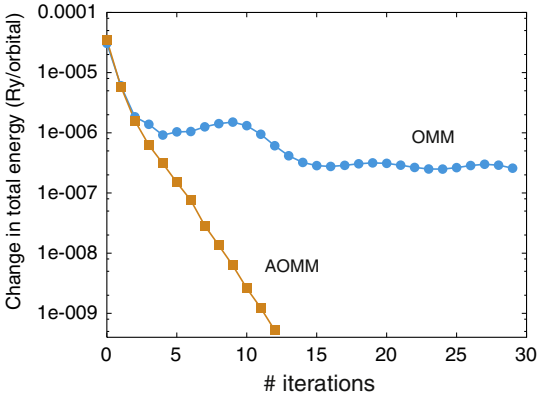

Figure 1. Convergence of ground state calculations for liquid water consisting of 125 molecules [42]. We used $R_{LR} = 12$ au in both calculations.

systematic convergence with respect to the number of basis functions. Furthermore, it is easy to achieve high performance on massively parallel computers with these basis functions. Therefore, the real space basis functions are ideal for the implementation of linear scaling methods. In this work, we investigate the properties of liquid ethanol from first principles with the help of linear scaling methods, together with finite-element basis functions.

2. Computational details

Our calculations are based on the DFT in the Kohn–Sham formalism [10, 11]. We used the generalized gradient approximation (GGA) in the Perdew–Burke–Ernzerhof (PBE) form [65]. The separable norm-conserving pseudopotentials [66–68] were employed, and only the Γ point was used to sample the Brillouin zone. The orbitals were expanded by finite-element basis functions of degree-3 [54, 55]. All production runs in the present paper were performed with an average cutoff energy [55] of 48 Ryd, while the resolution was approximately doubled at the positions of oxygen atoms by adaptation of the grids [52]. The atoms were treated classically, and the equations of motion for the atoms were integrated with the velocity-Verlet algorithm [69] using a timestep of 30 au (∼0.7 fs) in the production run. A Berendsen thermostat was used to control the temperature.

During the molecular dynamics simulations, the electronic states were quenched to the Born–Oppenheimer surface at every MD step with the limited-memory variant [70, 71] of the quasi-Newton method [72], which is more efficient than the conjugate gradient method [71]. The wavefunctions were extrapolated from previous MD steps [73]. The simulations were mainly performed on 108 AMD Opteron 2.0 GHz processors connected by Myrinet.

Liquid ethanol at ambient conditions was modeled by 125 molecules (1125 atoms, 1250 orbitals) in a cubic supercell of side 23 Å, which corresponds to the atomic number density measured at 298 K [74]. In order to study this system at reasonable computational cost, we relied on the orbital minimization method (OMM) [43–47], which is the most

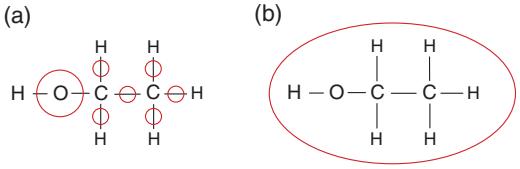

Figure 2. (a) Kernel regions for ethanol. (b) An alternative choice of kernel regions.

appropriate for our implementation among the various linear scaling methods. In OMM, each orbital is allowed to take nonzero values only in a given region of space, called the localization region (LR). It is common practice to choose the LRs so that each (localized) orbital can approximate the maximally localized Wannier functions (MLWFs) [75–77] as accurately as possible. Then, the computational cost of electronic structure calculations will grow only linearly with system size for a given accuracy. However, a naive implementation of OMM suffers from several drawbacks, such as the slow convergence problem [29, 30]. We have recently developed a novel algorithm, which we call the augmented orbital minimization method (AOMM) [42], to overcome these problems by imposing additional constraints on the orbitals. In the AOMM we first define the kernel regions (KRs) that are small (nonoverlapping) regions chosen to include the centers of MLWFs. These KRs allow us to eliminate the near redundancy of the orbitals, thus avoiding the problems mentioned above [42]. Figure 1 shows the convergence of ground state calculations in OMM and AOMM, clearly demonstrating the advantage of the latter.

In the current model, we have assigned seven spherical KRs (and LRs) to each molecule as illustrated in figure 2(a), where six KRs of radius $R_{KR} = 0.9$ au are centered at C–C and C–H bonds, each with a single orbital, and one KR of radius $R_{KR} = 1.2$ au is centered at an oxygen atom, with four orbitals. Although the latter can be split into four smaller ones, at least in principle, the centers of MLWFs around the oxygen atoms are too close to each other (compared to the grid resolution) to allow such a decomposition. Alternatively, we can construct each KR so that the whole molecule is included in a single KR, as shown in figure 2(b). This choice, however, leads to larger errors in total energy and atomic forces [42], and will not be used in this study. LRs are given by spherical regions of radius R_{LR} with the same centers as KRs, but boundaries of LRs are (slightly) modified to avoid interference with KRs [42].

Then, several trajectories of 0.5 ps in the microcanonical ensemble are used to evaluate the accuracy and performance of our implementation, as shown in table 1. Figure 3 shows the time evolution of total energies in these runs. In the conventional method, total energy drift is mainly caused by the use of a finite timestep for integration of the equations of motion and a finite tolerance for the ground state calculations. In the linear scaling calculations, additional errors arise from the fact that the boundaries of LRs and KRs change discontinuously as the atoms move, the effect of which is

Table 1. Simulation details for each run. ΔE denotes the relative error in total energy for the initial configuration. We used a timestep of 30 au and a tolerance of 10^{-9} Ryd/orbital for total energy minimization in all runs. Each MD step takes ≈10 min in (a).

	Method	R_{LR} (bohr)	Performance	ΔE	Drift (Ryd/atom ps)
(a)	$O(N^3)$	∞	1	0	2.9×10^{-5}
(b)	$O(N)$	8	8.0	1.43×10^{-4}	1.0×10^{-3}
(c)	$O(N)$	10	6.3	2.09×10^{-5}	3.0×10^{-5}
(d)	$O(N)$	12	4.6	3.20×10^{-6}	1.6×10^{-5}
(e)	$O(N)$	14	2.4	5.84×10^{-7}	1.8×10^{-5}

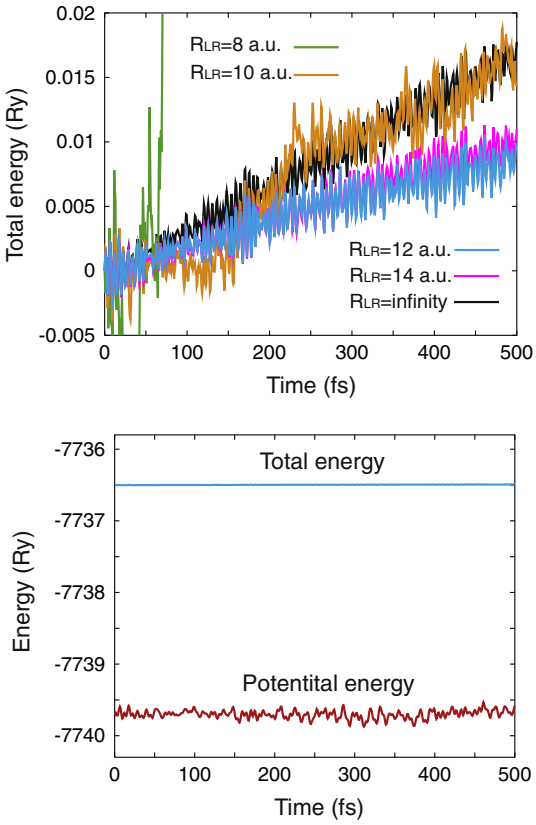

Figure 3. (a) Time evolution of the total energies for $R_{LR} = 8, 10, 12, 14$ au and ∞. The total energy of the initial step is chosen as the origin in all runs. (b) Time evolution of the total energy and potential energy for $R_{LR} = 12$ au.

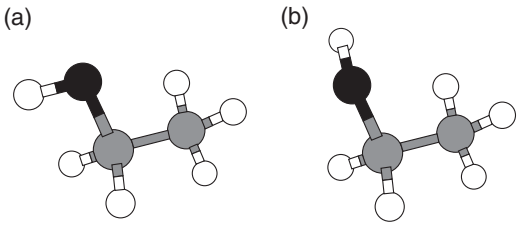

Figure 4. (a) *Trans* and (b) *gauche* conformers of ethanol.

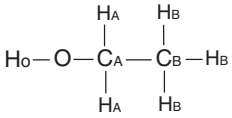

Figure 5. Notation for ethanol.

difficult to take into account analytically [42]. The last effect is prominent when $R_{LR} = 8$ au, and still persists to some extent when $R_{LR} = 10$ au However, we find excellent conservation for $R_{LR} = 12$ au, and a further increase to 14 au makes no improvement. Therefore, we used $R_{LR} = 12$ au in the production run as a good compromise between accuracy and speed, while R_{LR}s of 9–12 au were used in the equilibration runs.

Using these parameters, the system was first equilibrated for 25 ps at 1000 K, during which period all intramolecular covalent bond lengths were kept fixed with the RATTLE algorithm [78] to avoid dissociation. Then the temperature was gradually lowered to room temperature and all constraints on the bond lengths were removed. After another equilibration period of 7.5 ps, the statistics were collected during the production run of 10 ps at an average temperature of 299 K. No dissociation of the molecules occurred throughout the simulations.

3. Results

We first calculated the geometry of an isolated ethanol molecule to check the accuracy of our method. An ethanol molecule was placed in a cubic supercell of side 11.5 Å, and the equilibrium structures for the *trans* and *gauche* conformers (figure 4) were obtained by minimization of the total energy with respect to the atomic degrees of freedom using the quasi-Newton method [72]. No localization constraints were imposed on the orbitals. The calculated structural parameters are compared with other theoretical and experimental values in table 2, where the notation for the atoms is given in figure 5. Overall, our results are in satisfactory agreement with the reference values. Then, the intramolecular structural parameters of ethanol molecules in the liquid phase are averaged and compared with those of the isolated monomer in table 3. The only noticeable difference is the elongation of O–H bonds, which is caused by the formation of O–H$\cdots$O hydrogen bonds. Changes in the other parameters are much smaller than thermal fluctuations. Besides the parameters shown in table 3, each molecule has two rotational degrees of freedom. In particular, rotation of the O–H groups is an important reaction which is accompanied by a *trans/gauche* transition. We show the probability distribution of $\angle C_B C_A OH_O$ in figure 6. Integration of the distribution gives 61.0% of *gauche* and 39.0% of *trans* conformers, where each molecule is considered a *trans* conformer if $120° < \angle C_B C_A OH_O < 240°$,

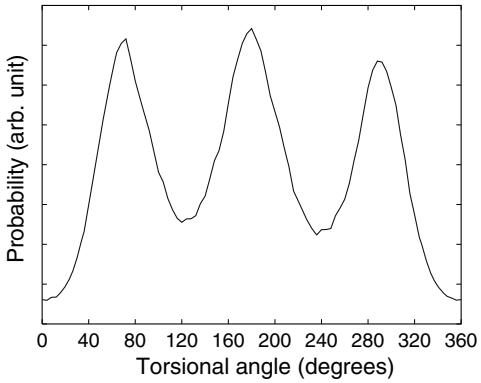

Figure 6. Probability distribution of the torsional angle around the O–C_A bond.

Table 2. Equilibrium structure of an isolated ethanol molecule. $r(C_A–H_A)$ and $r(C_B–H_B)$ denote the average values. Bond lengths are in Å and bond angles in degrees.

	This work	BLYP[a]	B_3LYP[b]	Experiment[c]
		Gauche		
r(O–H_O)	0.971	0.981	0.961	0.945
r(O–C_A)	1.435	1.455	1.429	1.427
r(C_A–C_B)	1.523	1.529	1.521	1.530
r(C_A–H_A)	1.102	1.100	1.092	1.094
r(C_B–H_B)	1.099	1.099	1.091	1.094
∠C_AOH_O	107.8	108.0	108.7	108.3
∠$C_B$$C_A$O	112.9	113.0	113.0	112.2
		Trans		
r(O–H_O)	0.969	0.980	0.960	0.945
r(O–C_A)	1.438	1.458	1.432	1.425
r(C_A–C_B)	1.516	1.523	1.515	1.530
r(C_A–H_A)	1.105	1.103	1.095	1.094
r(C_B–H_B)	1.098	1.098	1.090	1.094
∠C_AOH_O	108.0	108.4	109.0	108.3
∠$C_B$$C_A$O	107.9	107.6	108.0	107.2

[a] Reference [28].
[b] Reference [79].
[c] Reference [80].

and a *gauche* conformer otherwise. These results can be compared with the OPLS value of 50.0% for both conformers [2]. While statistical errors of our simulations are not negligible, as indicated by the asymmetry of the distribution, the major source of discrepancy is presumably the united atom and rigid body approximations in the OPLS force field. Meanwhile, rotation of the methyl groups around the C_A–C_B bonds occurs only on rare occasions, and will not be discussed here.

Now we proceed to the intermolecular structures. The radial distribution functions (RDFs) for selected atomic pairs are shown in figure 7. The characteristic features of these functions are the sharp first peaks of O–H_O and O–O RDFs, which are obviously due to the formation of O–H···O hydrogen bonds. The positions of these peaks are 1.75–1.80 Å for O–H_O and 2.75 Å for O–O, the latter being in satisfactory agreement with the experimental value of 2.8 Å [81]. These hydrogen bonds are also considered responsible for several other features, e.g. the first peaks of H_O–H_O and C_A–H_O RDFs. Overall, the OPLS force field [1–4] appears to give RDFs in nearly quantitative agreement with our results.

Table 3. The average structural parameters of ethanol molecules and their fluctuations in the liquid state. Δ denotes the differences from the gas phase values. Bond lengths are in Å and angles in degrees.

	Liquid	Δ
r(O–H_O)	0.991 ± 0.028	+0.021
r(O–C_A)	1.442 ± 0.033	+0.006
r(C_A–C_B)	1.526 ± 0.033	+0.006
r(C_A–H_A)	1.106 ± 0.030	+0.003
r(C_B–H_B)	1.102 ± 0.029	+0.003
∠C_AOH_O	108.5 ± 4.5	+0.6
∠$C_B$$C_A$O	111.6 ± 3.8	+0.7

Table 4. Hydrogen-bond statistics from our simulations, OPLS force field [2], and the polarizable version of OPLS [6] at ambient conditions. f_i is the fraction of molecules with i bonds, and $n_{HB} = \sum i f_i$.

	This work	OPLS	Polarizable OPLS
f_0	0.021	0.01	0.064
f_1	0.129	0.14	0.163
f_2	0.780	0.80	0.710
f_3	0.070	0.05	0.063
n_{HB}	1.90	1.9	1.77

Then, our RDFs have been utilized to evaluate the x-ray weighted radial distribution function which can be directly compared to the experimental one [81], as shown in figure 8. At first glance, our result appears to be significantly less structured than the experimental one, particularly at small r. However, at least part of the discrepancy is due to the numerical noise associated with Fourier transforms, as indicated by the behavior at $r < 2.5$ Å. In contrast, both functions are in excellent agreement with each other at large r (>6 Å) where the numerical noise plays only a minor role.

We have also carried out an analysis of hydrogen bonds based on the geometric criteria used in previous studies [2]: any intermolecular O···H_O pair is considered hydrogen bonded if (i) the O···H_O distance is less than 2.6 Å, (ii) the O···O distance is less than 3.5 Å, and (iii) the H_O–O···O angle is less than 30°, where the threshold values for the bond lengths also agree with the minima of our RDFs within statistical errors. The results of hydrogen-bond analysis from our simulations are compared with those of the previous studies in table 4. Our results suggest that the liquid phase of ethanol consists mainly of hydrogen-bonded chains, with occasional branching. We have also confirmed this view from the snapshots of simulations. The values from the OPLS force field are in much closer agreement with our results than those of the polarizable one.

The self-diffusion coefficient D of liquid ethanol was evaluated from the mean-square displacement of the molecular center of mass. The value of D from our simulation is 8.2×10^{-6} cm^2 s^{-1}, while the experimental value at ambient conditions is given by 1.1×10^{-5} cm^2 s^{-1} [82]. Since the statistical errors associated with the evaluation of D is relatively large, the agreement is considered reasonable.

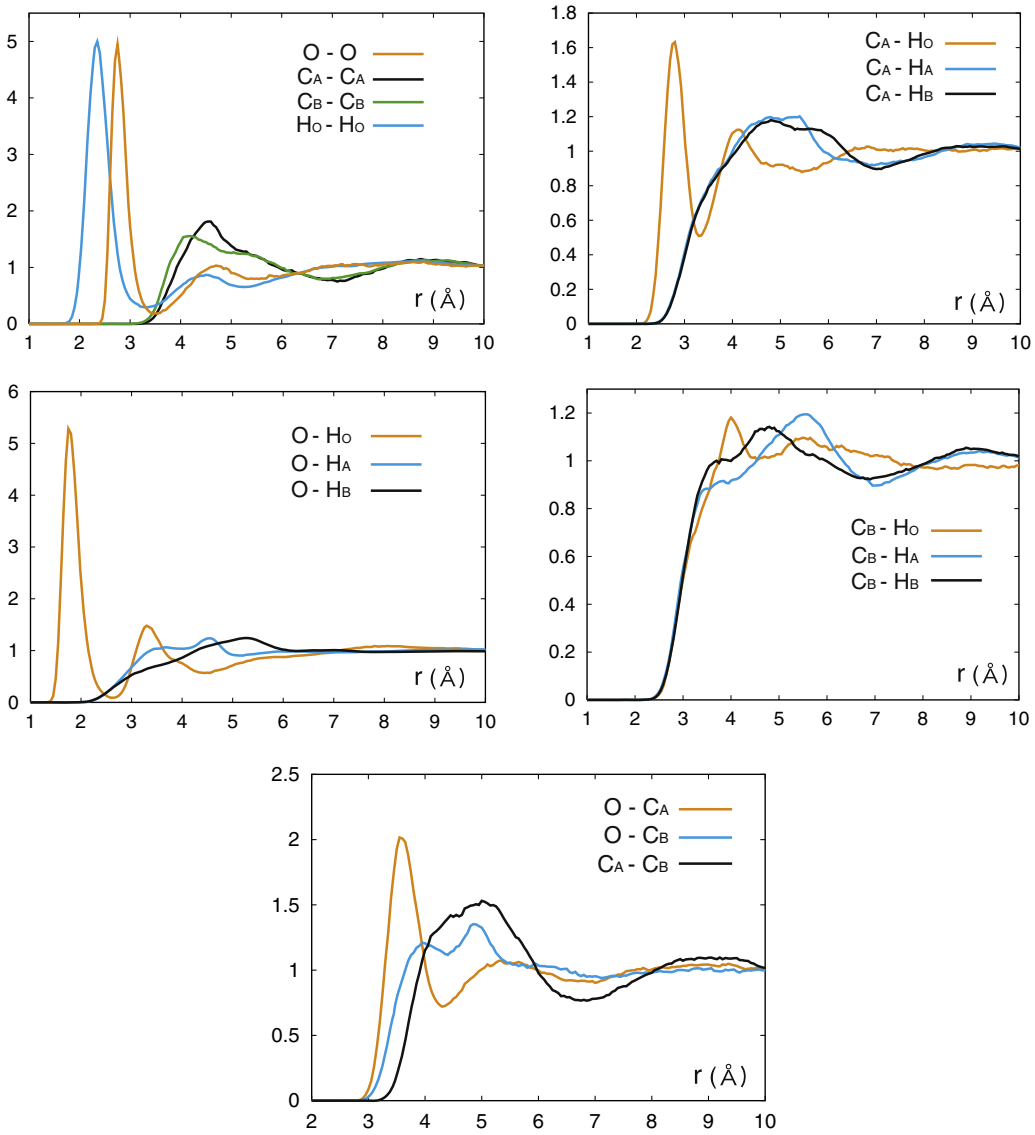

Figure 7. Intermolecular radial distribution functions for liquid ethanol.

Finally, the velocities of the atoms were used to estimate the vibrational density of states for the liquid phase, as shown in figure 9. The vertical lines denote the theoretical values for the isolated *trans* and *gauche* conformers. The highest frequencies, which correspond to the O–H stretch motion, are redshifted by $\sim$350 cm^{-1} with some broadening in going from the gas to the liquid phase. This effect, as well as the elongation of O–H bonds, is caused by the formation of the O–H$\cdots$O hydrogen bonds. The amount of redshift is in good agreement with the experimental value of 320 $\pm$ 10 cm^{-1} [79, 83, 84]. The rest of the frequencies are insensitive to the environment, which is consistent with the minor differences in the intramolecular structure shown in table 3.

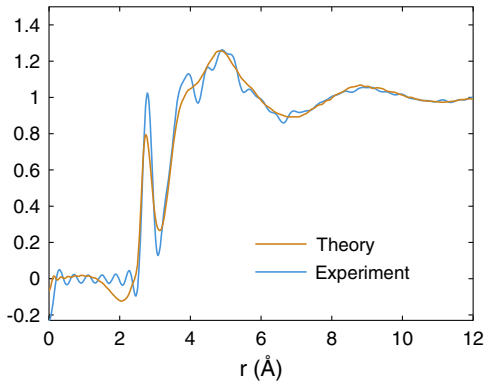

Figure 8. X-ray weighted radial distribution functions from theory (this work) and experiment [81].

4. Conclusion

The properties of liquid ethanol have been studied in detail from first principles. Good agreement with available experimental data was obtained for structural and dynamical properties. In particular, our results are consistent with the current understanding that liquid ethanol consists mainly of

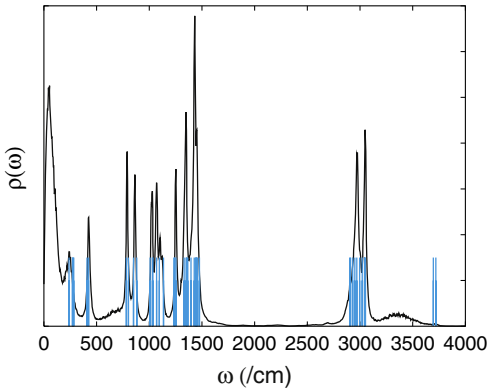

Figure 9. Vibrational density of states for liquid ethanol. Vertical lines denote the theoretical values for isolated *trans* and *gauche* conformers.

winding chains linked by O–H · · · O hydrogen bonds. We have found that the original OPLS force field provides structural properties in close agreement with our results, even though a relatively crude approximation is used for the intramolecular structure.

We have also shown that the use of a linear scaling algorithm based on AOMM reduces the computational cost of large scale *ab initio* molecular dynamics simulations significantly without sacrificing accuracy. We expect that our implementation will allow us to study huge systems that are otherwise intractable on the next generation of supercomputers.

The numerical data for figures 7, 8, and 9 are available as supplementary data files (available at stacks.iop.org/JPhysCM/20/294212).

Acknowledgments

The author would like to thank K Terakura and T Ozaki for fruitful discussions. This work is supported by the Next Generation Supercomputing Project, Nanoscience Program, MEXT, Japan.

References

[1] Jorgensen W L 1986 *J. Phys. Chem.* **90** 1276
[2] Saiz L, Padró J A and Guàrdia E 1997 *J. Phys. Chem.* B **101** 78
[3] Benmore C J and Loh Y L 2000 *J. Chem. Phys.* **112** 5877
[4] Petravic J and Delhommelle J 2003 *Chem. Phys.* **286** 303
[5] Gao J, Habibollazadeh D and Shao L 1995 *J. Phys. Chem.* **99** 16460
[6] González M A, Enciso E, Bermejo F J and Bée M 1999 *J. Chem. Phys.* **110** 8045
[7] Martín M E, Sánchez M L, Olivares del Valle F J and Aguilar M A 2002 *J. Chem. Phys.* **116** 1613
[8] Patel S and Brooks C L III 2005 *J. Chem. Phys.* **123** 164502
[9] Wang S and Cann N M 2007 *J. Chem. Phys.* **126** 214502
[10] Hohenberg P and Kohn W 1964 *Phys. Rev.* **136** B864
[11] Kohn W and Sham L J 1965 *Phys. Rev.* **140** A1133
[12] Car R and Parrinello M 1985 *Phys. Rev. Lett.* **55** 2471
[13] Martin R M 2004 *Electronic Structure: Basic Theory and Practical Methods* (New York: Cambridge University Press)
[14] Laasonen K, Sprik M, Parrinello M and Car R 1993 *J. Chem. Phys.* **99** 9080
[15] Sprik M, Hutter J and Parrinello M 1996 *J. Chem. Phys.* **105** 1142
[16] Diraison M, Martyna G J and Tuckerman M E 1999 *J. Chem. Phys.* **111** 1096
[17] Liu Y and Tuckerman M E 2001 *J. Phys. Chem.* B **105** 6598
[18] Boese A D, Chandra A, Martin J M L and Marx D 2003 *J. Chem. Phys.* **119** 5965
[19] Tsuchida E, Kanada Y and Tsukada M 1999 *Chem. Phys. Lett.* **311** 236
[20] Morrone J A and Tuckerman M E 2002 *J. Chem. Phys.* **117** 4403
[21] Handgraaf J W, van Erp T S and Meijer E J 2003 *Chem. Phys. Lett.* **367** 617
[22] Pagliai M, Cardini G, Righini R and Schettino V 2003 *J. Chem. Phys.* **119** 6655
[23] Handgraaf J W, Meijer E J and Gaigeot M P 2004 *J. Chem. Phys.* **121** 10111
[24] Tsuchida E 2004 *J. Chem. Phys.* **121** 4740
[25] Tsuchida E 2006 *J. Phys. Soc. Japan* **75** 054801
[26] Ikeda T, Boero M and Terakura K 2007 *J. Chem. Phys.* **126** 034501
[27] Choe Y-K, Tsuchida E and Ikeshoji T 2007 *J. Chem. Phys.* **126** 154510
[28] van Erp T S and Meijer E J 2003 *J. Chem. Phys.* **118** 8831
[29] Goedecker S 1999 *Rev. Mod. Phys.* **71** 1085
[30] Bowler D R and Gillan M J 2000 *Mol. Simul.* **25** 239
[31] Yang W 1991 *Phys. Rev. Lett.* **66** 1438
[32] Kitaura K, Ikeo E, Asada T, Nakano T and Uebayasi M 1999 *Chem. Phys. Lett.* **313** 701
[33] Soler J M, Artacho E, Gale J D, Garcia A, Junquera J, Ordejón P and Sánchez-Portal D 2002 *J. Phys.: Condens. Matter* **14** 2745
[34] Miyazaki T, Bowler D R, Choudhury R and Gillan M J 2004 *J. Chem. Phys.* **121** 6186
[35] Skylaris C K, Haynes P D, Mostofi A A and Payne M C 2005 *J. Chem. Phys.* **122** 084119
[36] Ozaki T 2006 *Phys. Rev.* B **74** 245101
[37] Subotnik J E, Sodt A and Head-Gordon M 2006 *J. Chem. Phys.* **125** 074116
[38] Nakano A *et al* 2007 *Comput. Mater. Sci.* **38** 642
[39] Rayson M J 2007 *Phys. Rev.* B **75** 153203
[40] Niklasson A M N and Weber V 2007 *J. Chem. Phys.* **127** 064105
[41] Wang F, Yam C Y, Chen G H, Wang X J, Fan K, Niehaus T A and Frauenheim T 2007 *Phys. Rev.* B **76** 045114
[42] Tsuchida E 2007 *J. Phys. Soc. Japan* **76** 034708
[43] Galli G and Parrinello M 1992 *Phys. Rev. Lett.* **69** 3547
[44] Kim J, Mauri F and Galli G 1995 *Phys. Rev.* B **52** 1640
[45] Ordejón P, Drabold D A, Martin R M and Grumbach M P 1995 *Phys. Rev.* B **51** 1456
[46] Fattebert J-L and Bernholc J 2000 *Phys. Rev.* B **62** 1713
[47] Fattebert J-L and Gygi F 2004 *Comput. Phys. Commun.* **162** 24
[48] Kohn W 1996 *Phys. Rev. Lett.* **76** 3168
[49] Chelikowsky J R, Troullier N, Wu K and Saad Y 1994 *Phys. Rev.* B **50** 11355
[50] Briggs E L, Sullivan D J and Bernholc J 1996 *Phys. Rev.* B **54** 14362
[51] Modine N A, Zumbach G and Kaxiras E 1997 *Phys. Rev.* B **55** 10289
[52] Gygi F and Galli G 1995 *Phys. Rev.* B **52** R2229
[53] White S R, Wilkins J W and Teter M P 1989 *Phys. Rev.* B **39** 5819
[54] Tsuchida E and Tsukada M 1996 *Phys. Rev.* B **54** 7602
[55] Tsuchida E and Tsukada M 1998 *J. Phys. Soc. Japan* **67** 3844
[56] Pask J E and Sterne P A 2005 *Modelling Simul. Mater. Sci. Eng.* **13** R71
[57] Yamakawa S and Hyodo S 2005 *Phys. Rev.* B **71** 035113
[58] Torsti T *et al* 2006 *Phys. Status Solidi* b **243** 1016
[59] Fattebert J-L, Hornung R D and Wissink A M 2007 *J. Comput. Phys.* **223** 759

[60] Hernández E, Gillan M J and Goringe C M 1997 *Phys. Rev.* B **55** 13485
[61] Haynes P D and Payne M C 1997 *Comput. Phys. Commun.* **102** 17
[62] Arias T A 1999 *Rev. Mod. Phys.* **71** 267
[63] Goedecker S and Ivanov O 1998 *Comput. Phys.* **12** 548
[64] Beck T L 2000 *Rev. Mod. Phys.* **72** 1041
[65] Perdew J P, Burke K and Ernzerhof M 1996 *Phys. Rev. Lett.* **77** 3865
[66] Kleinman L and Bylander D M 1982 *Phys. Rev. Lett.* **48** 1425
[67] Goedecker S, Teter M and Hutter J 1996 *Phys. Rev.* B **54** 1703
[68] Hartwigsen C, Goedecker S and Hutter J 1998 *Phys. Rev.* B **58** 3641
[69] Allen M P and Tildesley D J 1987 *Computer Simulation of Liquids* (Oxford: Oxford Science)
[70] Liu D C and Nocedal J 1989 *Math. Program.* **45** 503
[71] Tsuchida E 2002 *J. Phys. Soc. Japan* **71** 197
[72] Press W H, Teukolsky S A, Vetterling W T and Flannery B P 1992 *Numerical Recipes in Fortran* (Cambridge: Cambridge University Press)
[73] Arias T A, Payne M C and Joannopoulos J D 1992 *Phys. Rev. Lett.* **69** 1077
[74] El-Banna M M and Ramadan M Sh 1995 *J. Chem. Eng. Data* **40** 367
[75] Marzari N and Vanderbilt D 1997 *Phys. Rev.* B **56** 12847
[76] Berghold G, Mundy C J, Romero A H, Hutter J and Parrinello M 2000 *Phys. Rev.* B **61** 10040
[77] He L and Vanderbilt D 2001 *Phys. Rev. Lett.* **86** 5341
[78] Andersen H C 1983 *J. Comput. Phys.* **52** 24
[79] Coussan S, Bouteiller Y, Perchard J P and Zheng W Q 1998 *J. Phys. Chem.* A **102** 5789
[80] Sasada Y, Takano M and Satoh T 1971 *J. Mol. Spectrosc.* **38** 33
[81] Narten A H and Habenschuss A 1984 *J. Chem. Phys.* **80** 3387
[82] Hurle R L, Easteal A J and Woolf L A 1985 *J. Chem. Soc., Faraday Trans.* I **81** 769
[83] Shaw R A, Wieser H, Dutler R and Rauk A 1990 *J. Am. Chem. Soc.* **112** 5401
[84] Bonang C C, Anderson D J, Cameron S M, Kelly P B and Getty J D 1993 *J. Chem. Phys.* **99** 6245